Grounding topologies for resilient, integrated composite electrical power systems for future aircraft applications

Catherine E. Jones[1], Michal Sztykiel[2], Rafael Peña-Alzola[3], Patrick J. Norman[4] and Graeme M. Burt[5].
Institute for Energy and Environment, University of Strathclyde, Glasgow, UK G1 1XQ

The upwards trend for the use of electrical power on state of the art more-electric aircraft (MEA) has resulted in a significant changes to the electrical power system (EPS) for these platforms due to increased use of DC, higher voltage and power levels, and decentralized architectures. A dual trend is the increasing use of carbon fibre reinforced polymer (CFRP) for aircraft structures, due to the superior mechanical properties of CFRP compared to metallic structures. However, the poorer electrical conductivity of CFRP results in the aircraft structure no longer being fully integrated with the electrical power system. There is a need to integrate these two systems to fully maximize the performance benefits of CFRP, and optimize the weight and volume of the electrical power system. A first step in this integration is to identify an appropriate fault management strategy, which enables the detection of higher resistance ground faults through CFRP. This includes the consideration of appropriate grounding topologies. This paper proposes the implementation of a high resistance grounding topology, which enables the detection and location of a fault via spectral analysis of the voltage across the grounding resistor. From this, implications for wider EPS and CFRP designs to enable the reduction in the use of bulky cable harnesses, providing the first step to CFRP becoming an integral part of the EPS, are discussed.

I. Nomenclature

A	=	cross-sectional area *(m^2)*
C	=	Capacitance *(F)*
fo	=	actual motor frequency *(Hz)*
f_m	=	rated motor frequency *(Hz)*
I_{co}	=	Capacitive charging current *(A)*
I_f	=	Fault Current (A)
P	=	Electrical power (W)
P_{thresh}	=	Threshold electrical power (W)
R_{CFRP}	=	Electrical resistance of carbon fibre reinforced polymer (CFRP) *(Ω)*
R_F	=	Electrical fault resistance *(Ω)*
R_{HRG}	=	Electrical resistance of high resistance grounding (HRG) resistor *(Ω)*
V_{GPh}	=	Phase to ground voltage on generator feeder *(V)*
V_{LL}	=	Line to line voltage *(V)*
V_{LN}	=	Line to neutral voltage *(V)*
V_{MPh}	=	Phase to ground voltage on motor feeder *(V)*
V_{NG}	=	Neutral to ground voltage *(V)*
σ	=	Electrical conductivity *(Sm^{-1})*
ω	=	Angular frequency *(radians)*

[1] Research Associate, Department of Electronic and Electrical Engineering.
[2] Research Associate, Department of Electronic and Electrical Engineering.
[3] Research Fellow, Department of Electronic and Electrical Engineering.
[4] Senior Lecturer, Department of Electronic and Electrical Engineering.
[5] Professor, Department of Electronic and Electrical Engineering.

II. Introduction

The continued upwards trend for the use of electrical power on MEA, is resulting in on-board electrical power systems with higher voltage levels, increased use of direct current (DC) and more electrically powered critical loads [1]. In parallel to this there is a trend for the increased use of composite materials, in particular CFRP, for aero-structures, due to the superior mechanical performance of CFRP compared to metallic structures [2]. However, CFRP has a much poorer electrical conductivity than metallic structures [3][4] and hence cannot form part of the electrical return network on the aircraft, where the ground plane must have a low enough electrical resistance such that the voltage drop over the current return path is negligible [5][6]. To ensure that electrical current cannot pass through CFRP in the event of an electrical fault, extensive use of cable harnesses and raceways is made, with a current return network formed from existing metallic structures, with additional cables where necessary [7][8].

The methods used to ensure that CFRP cannot conduct electrical current mitigates to an extent the mechanical performance benefits attributed to the use of CFRP structures. Minimising the use of cable harnesses would not only reduce the significant weight and volume penalty that they attract, but would also reduce maintenance time for composite aircraft and engines [9]. A critical first step to enabling the development of integrated electrical power systems with CFRP is to enable the conduction of electrical current during faulted conditions, thus allowing the CFRP to form part of the path for electrical fault current, as shown in Fig. 1. However, the electrical resistance added to a fault path is known to be significantly higher than for a metallic material [10]. Existing standards require that an aircraft electrical power system is grounded using a TN-C-S grounding topology [11]. If the fault impedance added to the fault path by the CFRP is above 6.5 Ω, then this will result in a low electrical fault current that is difficult to detect [10]. Whilst this may not damage the wider electrical power system, it has been shown in [10] that the Joule heating in the CFRP from this fault current is significant, causing degradation to the CFRP structure.

Hence, the fault response of a ground fault through CFRP is influenced by a combination of the electrical resistance of the fault path, and the EPS architecture and grounding topology. Thus whilst it may be possible to control the electrical resistance added to the fault path by the CFRP by variation of layup [10], conductive additives [12] and method of electrically bonding to ground, this paper will explore the implementation of an alternative grounding topology and the interdependencies between this and the choice of EPS system design.

This paper will first discuss the theoretical interdependencies between fault response and different grounding topologies. Secondly the proposed grounding methodology to enable the integration of composites with the EPS on a MEA is demonstrated with a case study using a computer simulation of an example section of MEA network. From the results of the case study, the implications of the choice of grounding topology and resulting network fault response on the approach to fault management, including the choices surrounding the physical integration of CFRP with electrical ground and wider electrical power system design influences are discussed.

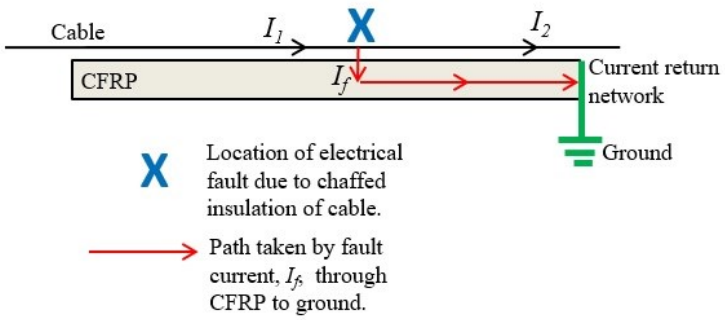

Fig. 1: Path of electrical fault current to ground through a CFRP panel mounted in a metallic frame which is electrically bonded to ground.

III. Interdependencies Between Fault Response and Grounding Topologies

A. Selection of an appropriate grounding topology

At present, aircraft electrical power systems are grounded using a TN-C-S: a 4 wire system, with a solidly grounded neutral point [13]. Due to the very low impedance of the grounding point, during a low resistance, short circuit to ground fault, high levels of fault current will flow. Whilst this will require a fast acting protection system to isolate

the fault, the high level of fault current enables the detection and location of the fault using conventional over-current or under-voltage based fault detection methods [10].

However, previous research by the authors [10] has demonstrated that the resistance added to the fault path of a solid rail to ground fault by CFRP can vary from 2.5 Ω to 25 Ω[10]. For a TN-C-S grounding topology, if the electrical resistance of a fault is less than 6.5 Ω, the DC link current will increase by at least 20% to feed the fault. The threshold for a 10% change in DC link current is 13.25 Ω. Therefore, the resistance of the CFRP may be too high to prevent a fault being detected in a TN-C-S system, but critically the fault current flowing through the CFRP may cause sufficient Joule heating that degradation of the CFPR occurs due to the glass transition temperature of the resin matrix of the CFRP being exceeded. A possible solution proposed in this paper is to consider a different grounding topology.

The response of an EPS with an ungrounded (IT) grounding system to a rail to ground fault is for a shift in the neutral voltage relative to ground, even for higher resistance faults. For example, in the case of a single phase to ground fault on a three phase section of network, the neutral point of the system will shift to the magnitude of the phase voltage, and the magnitude of the unfaulted phases will increase by a factor of $\sqrt{3}$ [13][14]. An additional advantage of this grounding topology is that for the case of a single line to ground fault, it allows for fault ride through capability. This approach to fault management may be particularly attractive for an aircraft EPS with critical loads.

Whilst this grounding topology offers fault ride through capability, the higher voltages on the unfaulted phases during a fault require that a higher level of voltage insulation is used [15]. The majority of faults in aircraft are caused by vibration and the resulting damage to cable insulation. Coupled with the trend for higher voltage levels on aircraft (set to continue for hybrid electric aircraft [16]), the level and type of insulation must be explored thoroughly. A second challenge of an ungrounded system is that it is rarely truly ungrounded due to capacitive connections to ground through parasitics (e.g. electrical machine casings) and EMC filters [17]. This results in high transient over-voltages during ground faults [13]

A third challenge of this grounding topology is that whilst a fault can be detected, it is known to be challenging to accurately locate where a fault has occurred on an ungrounded system [18]. This is critical for an aircraft EPS, as it is desirable to isolate only the faulted section of network to maintain power to critical loads. Sizing the system to operate at the higher voltages associated with a single rail to ground fault for a long period of time may be impractical, and secondly a fault must be located and isolated in a timely manner before a second rail to ground fault occurs.

Of these three key challenges, the first challenge, whilst important, is outside the scope of this paper. An option to mitigate against the second challenge of the transient over voltages is to use a high resistance grounding (HRG) topology. In a HRG topology the neutral point of the system is connected to ground via a grounding resistor. The resistor is sized to limit the ground current [13]. In the event of a line to ground fault occurring in a HRG system, the magnitude of the neutral to ground voltage will still shift to the phase (or DC rail) voltage. A method to locate a fault in an HRG system (the third challenge listed above) is critical to the implementation of this grounding topology for aircraft applications, and this is presented and discussed in Section III of this paper.

B. Application of HRG topology to an example MEA EPS

An example section of a more-electric aircraft EPS is shown in Fig. 2. In this system, a 236-kVA wound field synchronous generator provides variable frequency (360 – 800 Hz) voltage to a three phase, 230-V (rms) per phase bus. An autotransformer rectifier unit (ATRU) converts the AC voltage to +/- 270 V dc, with an inverter interfacing the DC link to an 80 kW permanent magnet synchronous motor (PMSM), which drives the environmental conditioning system (ECS). The parameters of the PMSM are given in Table 1.

The system has been modelled using a modular transient modelling tool [19]. As indicated in Fig. 2, the generator feeder cable to the ATRU has been modelled using a lumped parameter model [20] to represent the bundled phase and neutral cables. The current return network impedance has been represented by a lumped impedance of 2mΩ and 8 mH [2]. There is a capacitive coupling between the cable sheath and ground (1.2 nF per phase), which will conduct stray currents generated by electromagnetic interference [21]. In addition, there is capacitive coupling between the generator casing and ground (0.1 μF per phase). Downstream of the system, the DC section of network, active inverter and motor are not connected to neutral. This is to isolate AC and DC grounds.

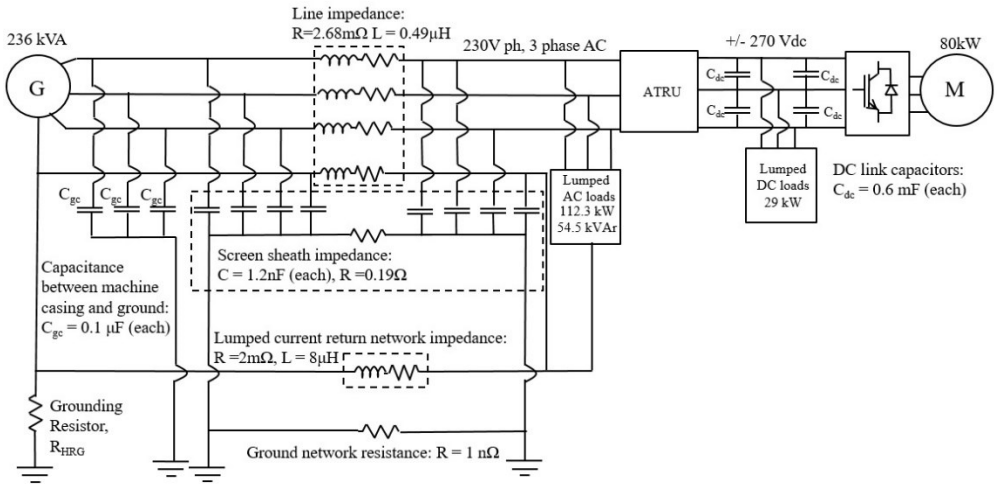

Fig. 2: Example EPS architecture with HRG

Table 1: ECS motor parameters

Parameter	Value for PMSM
Stator Resistance	5 mΩ
Stator d-axis Inductance	75 μH
Stator q-axis Inductance	77 μH
Stator 0-seq. Inductance	0.1 mH
Number of Pole Pairs	5
Voltage Constant *Ke*	22 V/krpm
Inertia	2.02 x 10^{-4} kg m^2

To implement the HRG grounding topology, a neutral point of the system must be grounded through a grounding resistor. For the system shown in Fig. 2, the star point of the generator is grounded through a grounding resistor. The resistor is sized to ensure that the ground fault current is greater than the capacitive charging current, such that transient over voltages are avoided in the event of a fault. Using (1) and (2) from [13], where I_{co} *(A)* is the charging current, V_{LL} *(V)* is the line to line voltage, V_{LN} (V (rms)) is the line to neutral voltage, f (Hz) is the fundamental frequency, C_o *(F)* is the value of the total parasitic ground capacitance, the grounding resistor, R_{HRG}*(Ω)*, can be sized.

$$3I_{co} = 2\sqrt{3}\, V_{LL}\pi f C_o \tag{1}$$

$$R_{HRG} = \frac{V_{LN}}{3I_{co}} \tag{2}$$

By inspection of Fig. 2, there are two sets of capacitors which must be considered when implementing (1): the capacitance between the machine casing and ground, and between the cable sheath and ground. At present the system has only been modelled in simulation and therefore other parasitic capacitive connections to ground, for example from casings or heat sinks [22] have been overlooked. Common mode electromagnetic coupling (CM EMC) filters have also not been included. The design of the CM EMC filter is dependent on a number of factors including converter topology and switching frequency[22], and depending on its design, it may affect fault response and sizing of R_{HRG}.

In the modelled system, the phase voltage is 230 V (rms) and the coupling capacitance to ground is 0.1 μF (the coupling capacitance due to the cable sheath is neglected as it is significantly smaller than the coupling capacitance due to the generator casing). By inspection of (1) and (2) system frequency directly influences the sizing of R_{HRG}. The frequency of the generator feeder can vary from 360 – 800 Hz [23]. If designed for a 400 $V_{LL\ (rms)}$ voltage at 800 Hz, the resistor will be 660 Ω, for 360 Hz it is 1467 Ω, or for a nominal 400 Hz it is 1320 Ω. Selection of a higher voltage level may result in a higher value for R_{HRG}, as well as higher insulation requirements during a rail to ground fault. Clearly a larger resistor brings a higher associated weight penalty. However, this penalty may be minimal when

traded against the value of implementing higher voltage (lower resistive losses) and variable frequency (to enable matching of generator and engine speed).

IV. Method of fault detection

A. Appropriate Method of Fault Detection and Location Method for an MEA EPS

The attraction of a HRG grounding topology for an integrated electrical composite system is that a ground fault can be detected by a voltage shift between a neutral point and electrical ground. However, due to the low fault current associated with first ground faults in HRG systems, locating where a fault has occurred is not straight forwards: classical methods of fault detection include the injection of a traceable signal into a faulted system, and to then use this to trace the fault by hand [18]. A second method is to gradually de-energise the system to locate the fault [18]. Clearly for an aircraft where a fault occurs during flight, these approaches would be impractical as both can only take place once the aircraft is stationary on the ground. Even if fault current levels from a rail to ground fault are too low to cause thermal degradation to CFRP, a timely detection and isolation of a rail to ground fault is required to ensure that a fault is cleared before a second rail to ground fault occurs.

Analysis of the neutral to ground voltage measured over the grounding resistor, R_{HRG}, has been proposed in the literature for land-based systems with adjustable speed drives (ASD) [24][25]. By analysis of the magnitude and frequency of this measured voltage, the location of a fault can be estimated. Three fault locations in the MEA EPS in Fig. 2 are considered, as indicated in Fig. 3. Each fault is a single phase, or rail, to ground fault, through CFRP. By inspection of Fig. 3, the voltage over R_{HRG} for each of the three fault locations can be expressed by Equations (3) – (5) [24],[25] in Table 2, where $\overline{V_{GPh}}$ *(V)* is the generator feeder phase to ground voltage, R_f *(Ω)* is the fault resistance, V_{dc} *(V)* is the rail to ground DC link voltage, f_o *(Hz)* and ω_0 (rad/s) is the actual frequency of the AC motor feeder voltage, f_m *(Hz)* is the rated frequency of the AC motor feeder voltage, $\overline{V_{MPh}}$ *(V)*, and ϑ_0 *(rad)* is the phase difference of the motor feeder voltage.

By inspection of (3) – (5) it is clear that frequency spectra analysis of the neutral to ground voltage offers an opportunity to detect and locate a higher resistance fault through CFRP on an HRG system: the dominant frequency of the measured V_{NG} is the frequency of the faulted section of the network. In this paper the spectral analysis of the voltage has been carried out using a Fast Fourier Transform (FFT), over a sample period of 0.1 ms.

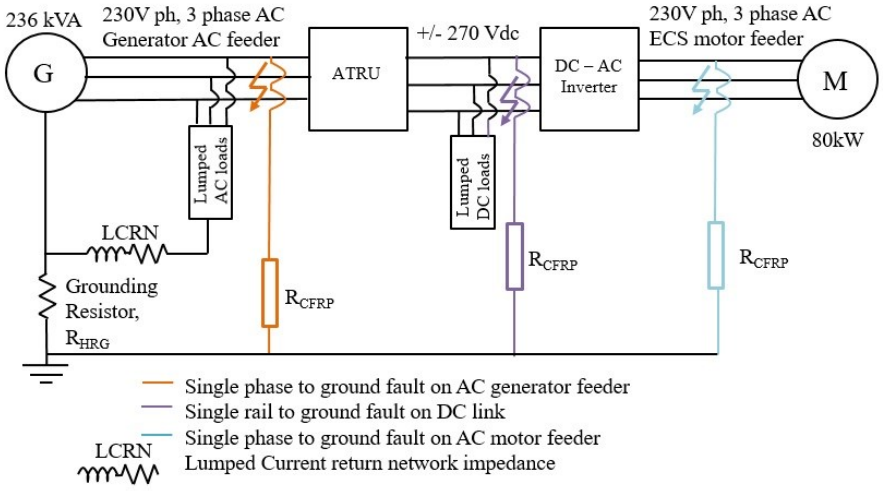

Fig. 3: Location of 3 ground faults under consideration for EPS with HRG topology

Table 2: Theoretical voltages over R_{HRG} during a rail to ground fault at different locations in the network.

Location of fault	Neutral to ground voltage
Generator feeder	$\overline{V_{NG}} = -\frac{R_{HRG}}{R_{HRG}+R_f}\overline{V_{GPh}}$ (3)
DC link	$\overline{V_{NG}} = -\frac{R_{HRG}}{R_{HRG}+R_f}V_{dc}$ (4)
Motor feeder	$\overline{V_{NG}} = -\frac{R_{HRG}}{R_{HRG}+R_f}\frac{f_0}{f_m}V_{MPh}\sin(\omega_0 + \vartheta_{0)}$ (5)

B. Variation of Fault Resistance

In each of the fault scenarios and resulting neutral to ground voltages given in Table 2, the magnitude of the resulting neutral to ground voltage is dependent on the ratio of R_{HRG} to the sum of R_{HRG} and R_f, where R_f is dominated by the resistance of the CFRP, R_{CFRP}. CFRP is a heterogeneous material where carbon fibres, which provide the strength, are held in place by a resin matrix. The resin matrix is usually a thermoset epoxy. Carbon fibre is an electrical conductor, whereas the resin matrix is an electrical insulator. The carbon fibres are arranged in plies. Within each ply the carbon fibre may be arranged in a unidirectional (UD) (strands parallel to each other) or woven fashion [26]. The orientation of the fibres relative to different plies is varied to give appropriate mechanical properties to the CFRP.

However, the electrical properties of the CFRP are also dependent on the lay-up of the CFRP [10]. It has been shown in previous work by the authors [4][10] that the electrical resistance of UD CFRP can be estimated based on

$$R = \frac{l}{\sigma A}(\Omega) \tag{6}$$

where R (Ω) is electrical resistance, l (m) is the length of CFRP that is conducting, σ (Sm^{-1}) is the electrical conductivity of the CFRP in the in-fibre direction and A is the cross-sectional area of CFRP that is conducting. In [10], for a 0.65 m x 0.65 m square panel of UD CFRP, bonded to ground via a metallic frame, the electrical resistance added to the fault path in a solid short circuit fault was estimated to vary from ~2.5 Ω to ~ 25 Ω.

If the grounding resistor is sized for a generator feeder frequency of 800 Hz (minimizing the size of R_{HRG} thus maximizing the impact that a change R_{CFRP} will have on neutral voltage under fault conditions), then the magnitude of the phase to neutral voltage will vary from a reduction of 1% of the system voltage with an R_{CFRP} of 2.5 Ω, to a reduction of 4% of the system voltage for an R_{CFRP} of 25 Ω. Therefore, aside from providing information on the location of a fault, the magnitude of the frequency spectra are expected to be sufficiently higher than any noise on the ground plane to enable the detection of a fault.

V. Analysis of Fault Response

A simulation model of the section of MEA EPS shown in Fig. 2 was created in Matlab Simulink, and single phase to ground faults were applied to the three locations indicated in Fig. 3: phase A of the generator feeder, the positive rail of the DC link and phase A of the motor feeder. In all three cases the maximum fault resistance identified in [10] a fault of of 25 Ω was applied, and R_{HRG} was sized to be 1320 Ω, for the nominal generator feeder frequency of 400Hz.

A. Voltage Response to a Single Rail to Ground Fault

Fig. 4 shows the response of the phase to ground voltages in response to a phase A to ground fault after 0.5 s. Fig. 5 shows the voltage measured between neutral and ground over R_{HRG}. By inspection it is clear that in response to the fault, the phase to ground voltages of the unfaulted generator feeder phases increase by a magnitude of $\sqrt{3}$ to a peak of 563 V (400 V (rms)). The neutral voltage increases to a peak voltage of 320 V, which corresponds to the expected magnitude from (3). Fig. 6 shows the generator feeder phase to ground voltages when the positive rail of the DC link

is shorted to ground after 0.5 s. The downwards shift of the voltage magnitudes relative to ground is due to the downwards shift of the neutral voltage relative to ground, shown in Fig. 7. The magnitude of the neutral to ground voltage over R_{HRG} is ~265 V, which corresponds to the value estimated using (4).

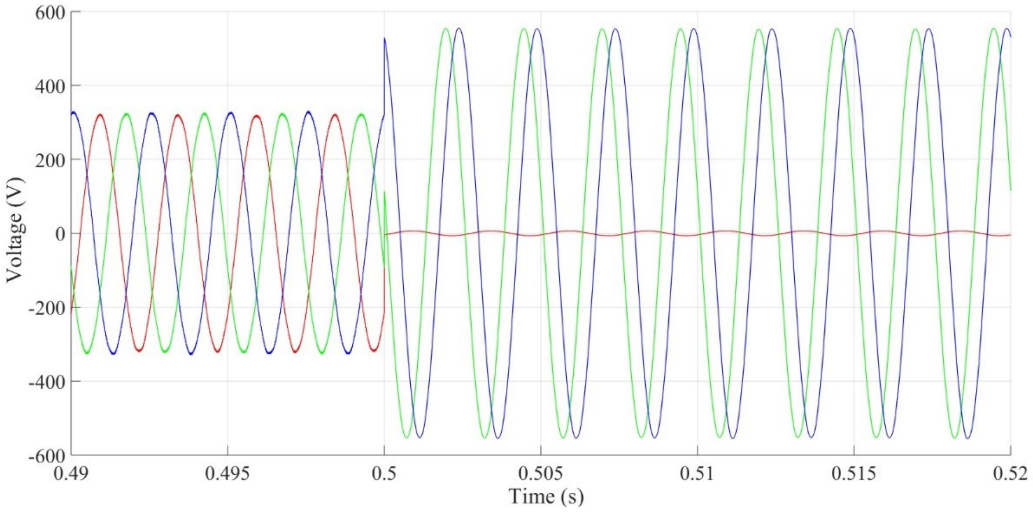

Fig. 4: Generator feeder phase to ground voltages with phase A (red) to ground fault applied to the generator feeder after 0.5s, and unfaulted phase B (green) and C (blue) increasing in amplitude by a factor of √3 in response to the fault.

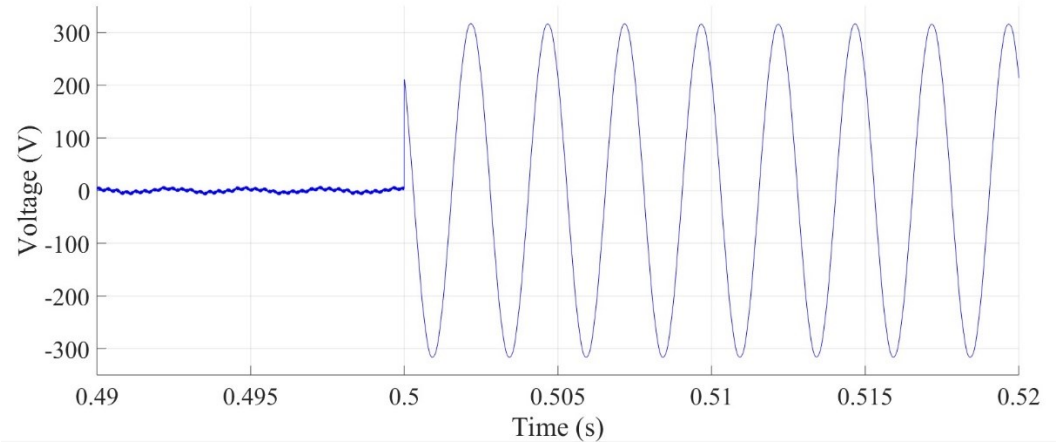

Fig. 5: Neutral to ground voltage (measured over the R_{HRG}) with a Phase A to ground fault applied to the generator feeder after 0.5 s.

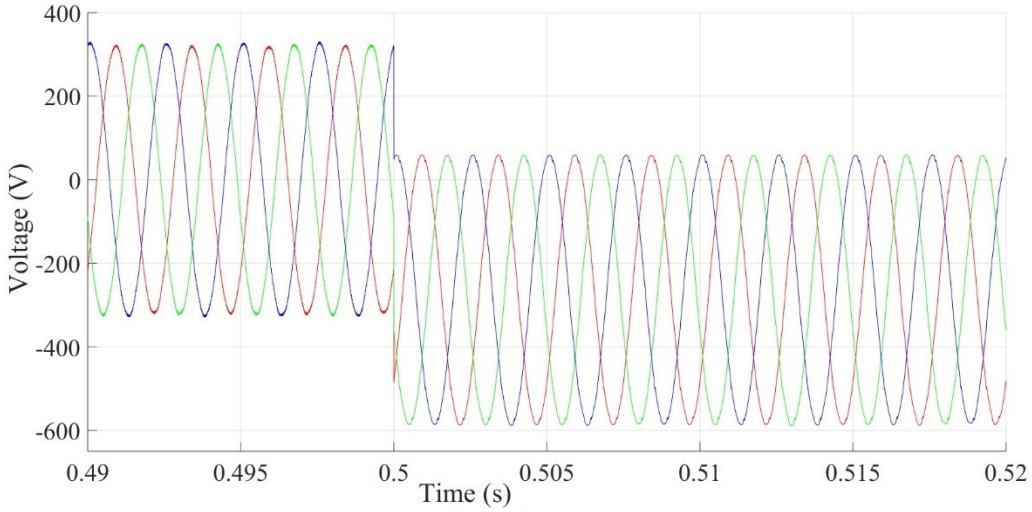

Fig. 6: Generator feeder phase to ground voltages (Phase A in red, Phase B in green, Phase C in blue) with positive rail to ground fault applied to the DC link after 0.5 s.

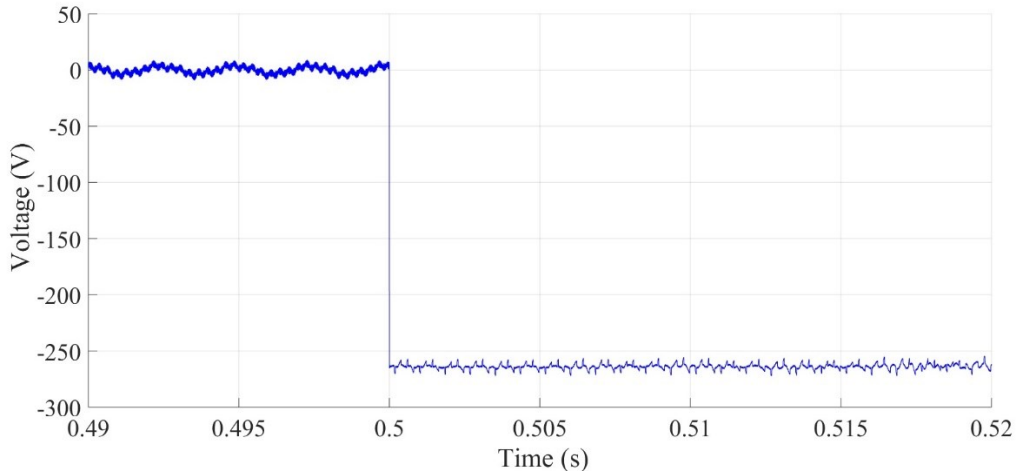

Fig. 7: Neutral to ground voltage, V_{NG}, (measured over R_{HRG}) with a positive DC rail to ground fault after 0.5s.

To investigate the fault response to a motor feeder phase to ground fault, if the EPS is simplified to the system shown in Fig. 8 where the ATRU is represented simply by a diode bridge rectifier, and the inverter by an ideal six switch converter, then when switch S1 closes, fault current (I_F) will flow directly from the positive DC link rail to ground via R_{CFRP}. Due to R_{HRG}, this current will flow back through the generator and diodes D1, D3 and D5 (in Fig. 8 D1 is commutated on by the phase A generator voltage). When S2 closes, the path will change to link the negative DC link rail to ground, with D2, D4 and D6 conducting. Therefore under this fault condition, the voltage on the faulted phase will go to ground, and the phase to ground voltage over the 2 unfaulted phases will increase by $\sqrt{3}$. The voltage measured over R_{HRG} (Fig.9) appears to have a magnitude of the DC link voltage. Further, the generator phase to ground voltages maintain their fundamental waveform, but with a superimposed voltage at +/- 270V (the DC link voltage) (Fig. 10). Finally, the switching of the positive and negative DC rail voltages between +270 Vdc and – 270 Vdc, and how this impacts on V_{NG} is shown in Fig.11.

Fig. 12 shows the spectral analysis of the neutral to ground voltage over the grounding resistor using a Fast Fourier Transform (FFT), over a sample period of 0.1 ms for each of the three fault scenarios. The position of the spectra aligns with the fundamental frequency of the section of network where a fault has occurred, thus enabling the location of a fault to be detected.

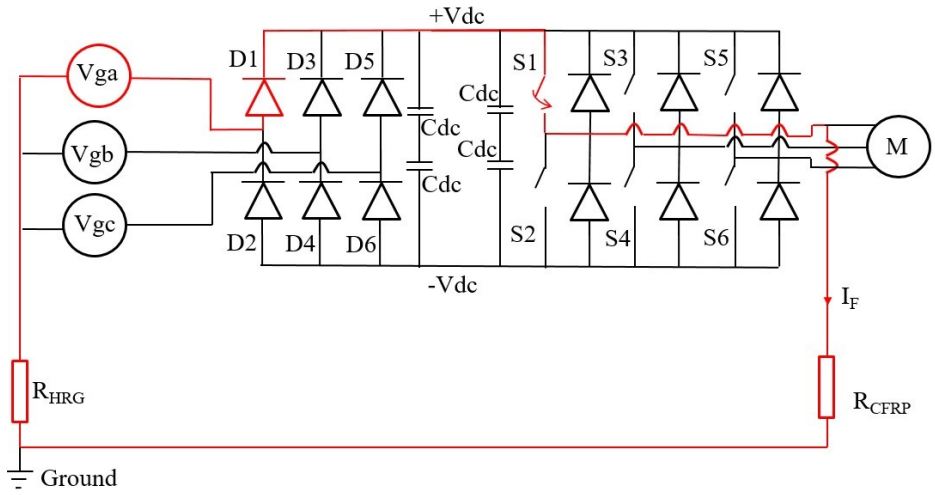

Fig. 8: Simplified system diagram to indicate fault current path during a phase A to ground fault on the motor feeder. The red path indicates the conduction path when S1 closes.

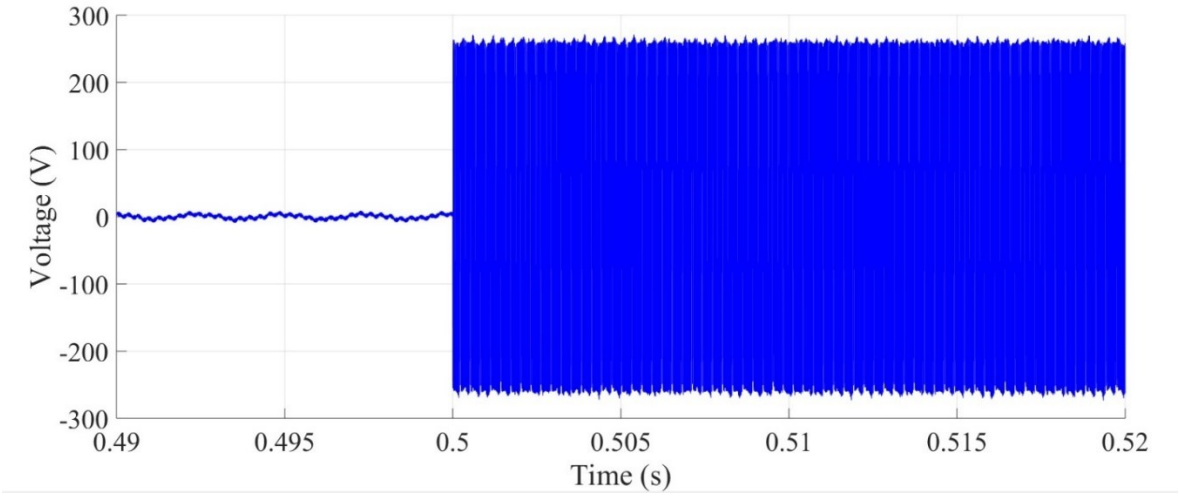

Fig. 9: Neutral to ground voltage, V_{NG}, (measured over R_{HRG}) with a Phase A to ground fault applied to the motor feeder after 0.5 s.

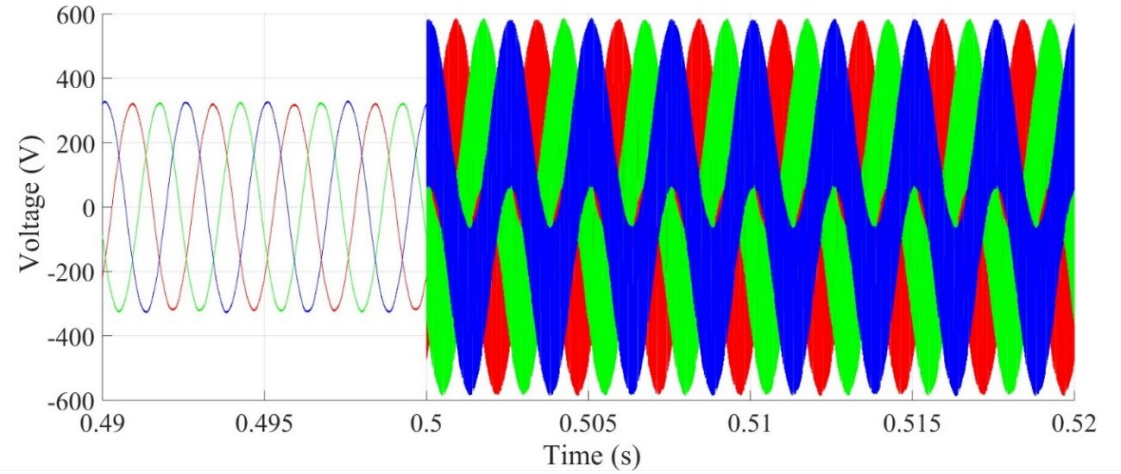

Fig. 10: Generator feeder phase to ground voltages with a phase A to ground fault applied to the motor feeder after 0.5s.

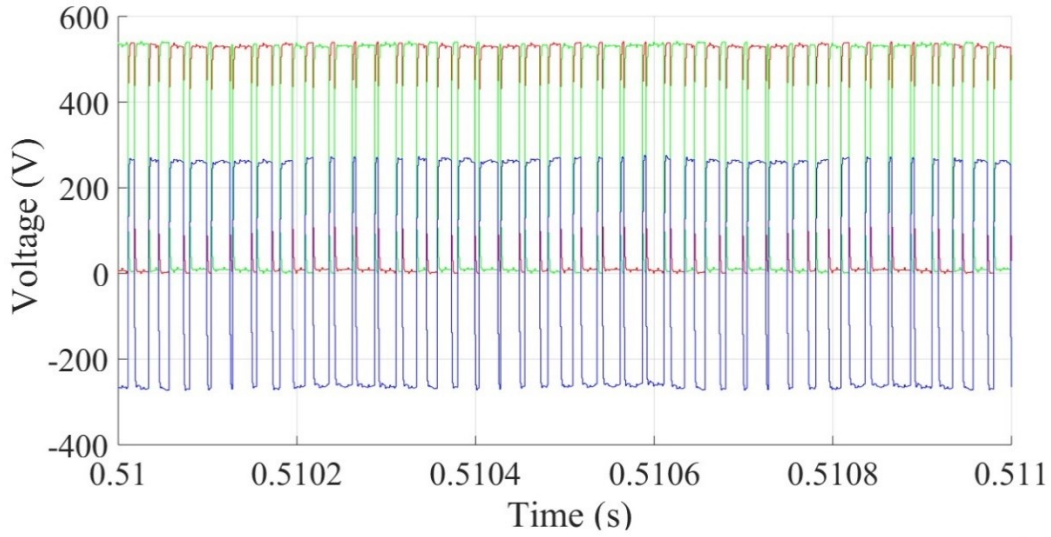

Fig. 11: +270 V DC link rail to ground voltage (red), -270 V DC link rail to ground voltage (green) and voltage over R_{HRG} when a phase A to ground fault has been applied to the motor feeder after 0.5 s.

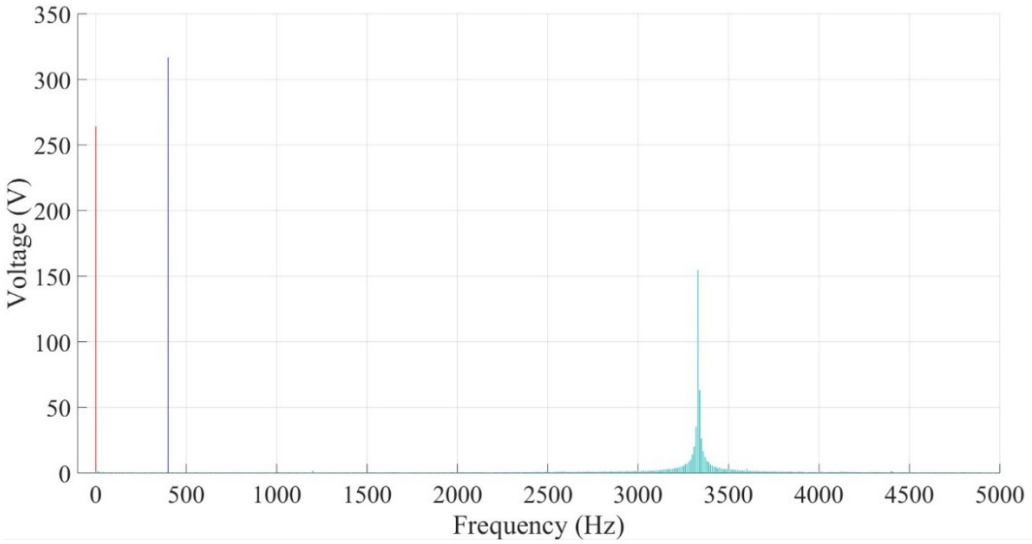

Fig. 12: Spectral analysis of the neutral to ground voltage over the grounding resistor, where blue is for a single phase of the generator feeder to ground, red is for the positive rail of the DC link to ground and cyan is for a single phase of the motor feeder to ground.

B. Fault Current Through CFRP

From [10] it is known that the injection of electrical current through CFRP will result in localized Joule heating. The amount of power dissipated in a section of CFRP is expressed as

$$P = I_f^2 R_{CFRP} \tag{7}$$

where *P (W)* is the power dissipated (usually as heat), I_f *(A)* is the fault current flowing through the CFRP and R_{CFRP} *(Ω)* is the electrical resistance of the CFRP. The amount of fault current can be estimated by (8), if it is assumed that the combined R_{HRG} and R_{CFRP} resistances dominate system impedance such that the resistance of the EPS, including electrical machines, can be considered negligible. For example, if an AC feeder single phase to ground fault is considered then the combined grounding and fault resistance dominates system impedance, hence the stator windings of the machine are neglected, as is the coupling capacitance to ground. Hence the fault current can be estimated from

$$I_f = \frac{V_{ph}}{R_{HRG}+R_{CFRP}} \tag{8}$$

For the case considered, the fault current through the CFRP is 0.335 A(rms) if the grounding resistor is sized for the maximum generator feeder frequency of 800 Hz, or 0.171 A(rms) if sized for 400 Hz, in both cases with R_{CFRP} at the highest expected value of 25 Ω, as shown in Fig. 13. The initial transient is due to the discharge of the parasitic capacitances (generator casing and cable sheath) included in the model. It must be noted however, that no equivalent series resistance (ESR) has been included in series with the capacitors. From (7), this would lead to a power dissipation in the CFRP of 2.8 W (R_{HRG} at 660 Ω) or 0.074 W (400Hz). From the guidance given in [10][4], it can be assumed that this is not sufficient power dissipation to cause Joule heating to raise the temperature of the conducting CFRP to above the glass transition temperature of the resin.

Similarly, in the case of a DC link rail to ground fault, the power dissipated in the CFRP will be 1 W with R_{HRG} at 1320 Ω, and 3.88 W at 660 Ω. At 3.88 W, the glass transition temperature of the resin could be reached, but it will take several hours and is dependent on environmental conditions, including any natural cooling of the CFRP.

From (7) and (8) the calculated fault current through the CFRP in the case of a motor feeder single phase to ground fault is calculated to be the same as for the generator feeder fault, if the system is operating at the same nominal voltage. However, the high frequency switching that is present on the fault current results in the parasitic capacitances to ground discharging every time the voltage switches. Further experimental investigation is required to understand how this affects the thermal response of the CFRP. If the current is averaged at 2A, then the power dissipated would be 100 W, which would be sufficient heating to reach glass transition temperature in ~3s, but if the average current is

1A, then the power dissipated is 50 W, which would reach glass transition temperature in ~20s [10]. In both cases the time to reach glass transition temperature assumes no natural cooling of the CFRP is present.

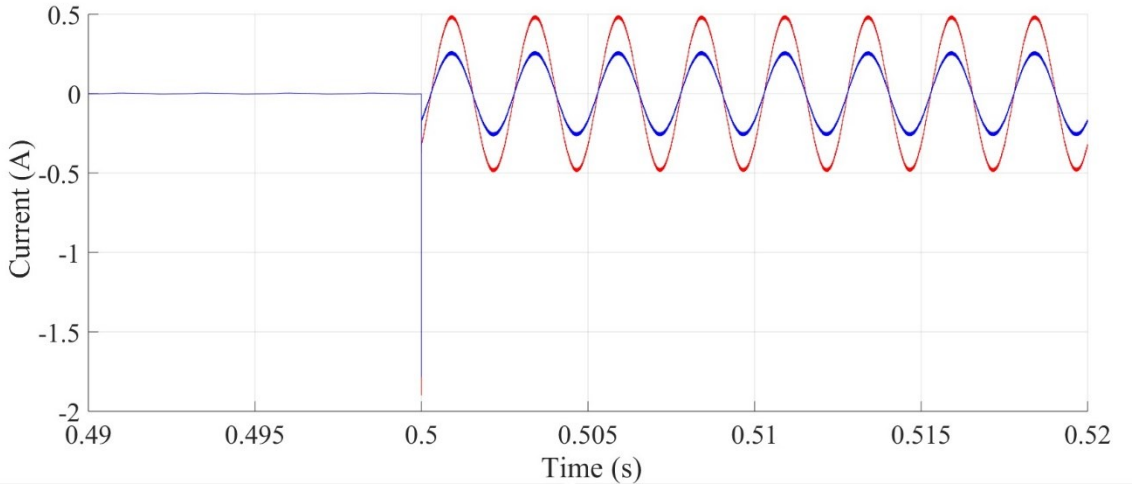

Fig. 13: Measured fault current through the CFRP for a generator feeder phase A fault to ground, with R_{HRG} is 660 Ω and R_{CFRP} is 25 Ω (red), R_{HRG} is 1320 Ω and R_{CFRP} is 25 Ω (blue)

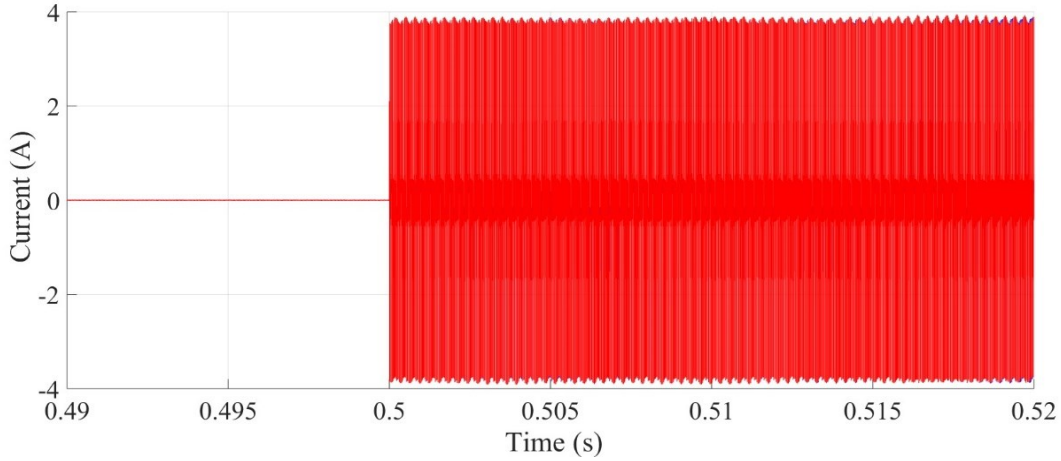

Fig. 14: Measured fault current through the CFRP for a motor feeder phase A fault to ground, R_{HRG} is 660 Ω and R_{CFRP} is 25 Ω (red), R_{HRG} is 1320 Ω and R_{CFRP} is 25 Ω (blue)

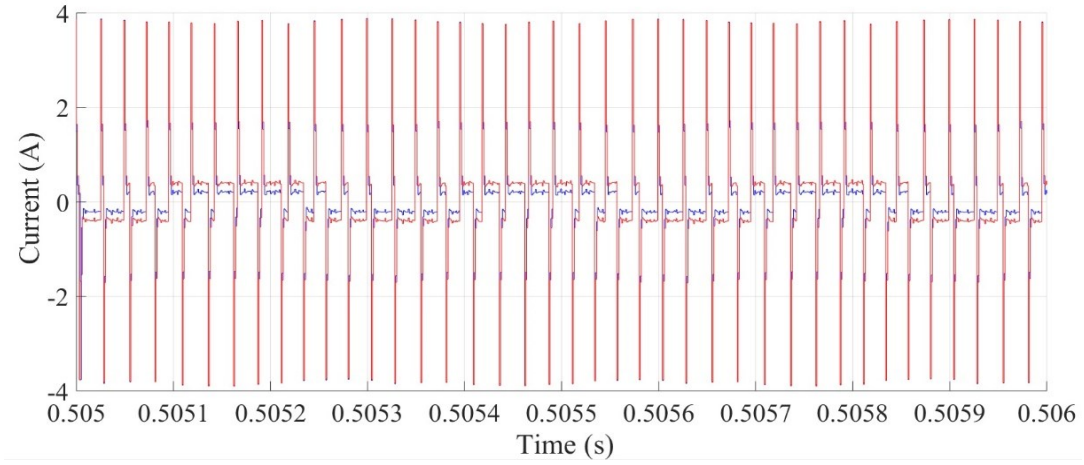

Fig. 15: Zoomed in over a period of 1 ms for the measured fault current through the CFRP for a motor feeder phase A fault to ground, R_{HRG} is 660 Ω and R_{CFRP} is 25 Ω (red), R_{HRG} is 1320 Ω and R_{CFRP} is 25 Ω (blue)

VI. Discussion

A. Influences of Grounding Topology Choice on Wider EPS Design

From the case study results shown, it can be seen that the HRG topology provides a method to detect a higher resistance ground fault through CFRP. The use of a high resistance grounding topology has an additional benefit to the system of providing fault ride through capability. Aero-electrical power systems have increasing numbers of critical loads, and hence HRG provides an additional option for designing a system with an appropriate fault management strategy to ensure power to such loads is maintained. This is very relevant to the design of the EPS for future hybrid-electric aircraft, where some of the thrust for the aircraft may be from electrically driven fans [16].

However, as the results indicate, an HRG topology does require an electrical power system to be able to withstand higher voltage levels during faulted conditions. This has several implications system design. Firstly, the cables will require appropriate levels of cable insulation and repeated higher voltages can lead to degradation of the cable insulation due to high voltage stress [29]. Secondly, the components within the system must be rated to cope with higher voltage levels. This may require the use of multilevel converter topologies, such as neutral point clamped converters [27]. Such converter topologies also have improved power quality and efficiency compared to 2-level topologies [28].

A second consideration must be the influence of the converter and filter topologies on the over-voltage levels experienced during a fault. For example, in the case study shown, the use of a six switch converter resulted in a switching voltage with a magnitude of the rail to rail DC link voltage being superimposed on top of the generator feeder AC phase voltage. The choice of appropriate converter topologies (including the use of galvanic isolation) to mitigate these over-voltage responses is an area for future discussion.

A further consideration which has not been fully explored in the case study is the full influence of common mode capacitive coupling to ground on the fault response. This includes common mode filters and coupling capacitances due to other elements such as heat sinks or the casing of the equipment in the EPS to ground. Combined with the EPS system architecture, these common-mode connections will influence the common-mode current which will flow in response to a fault to ground. Further study is required to understand the frequencies and magnitudes of these circulating currents. If the casing of any of the EPS technologies is made from CFRP, as is proposed by [9], then how the design of these casings affects the capacitive coupling to ground and the common-mode currents needs to be understood. Furthermore, the interdependencies between CFRP layup and bonding to ground and the thresholds for common-mode current and voltage magnitude and frequency for degradation of the CFRP require characterization.

B. Interdependencies Between Fault Resistance and High Resistance Grounding Resistor

From the results for the example system described in Section IV, it can be observed that the level of power dissipated in the CFRP is not high enough to cause sufficient Joule heating of the CFRP for the glass transition temperature of the CFRP to be reached (assuming the average current in response to a motor feeder to ground fault is below 1A). However, if the power dissipated in the CFRP is ~80 W or higher, glass transition temperature will be reached within a few seconds. This sets a maximum acceptable fault current of 1.7 A (with R_{CFRP} at 2.5 Ω). If a design criteria for the system is selected that limits the power dissipated in the case of a fault to a specific power level, then this will influence the choice of wider system parameters. The threshold power, $P_{thresh,}$ is determined by (9).

$$P_{thresh} \leq I_f^2 R_{CFRP} \tag{9}$$

The level of P_{thresh} will be influenced by the expected speed of response of the fault detection and protection system, and the acceptable levels of localized heating in the environment around a section of CFRP due to a fault. From the limit for I_f from (9) a limit for the grounding resistor is set, which with consideration of (2) the allowable charging current can be calculated. By inspection of (1) it can be seen that the charging current is a function of system voltage, frequency and the coupling capacitance to ground. How much flexibility there is to vary these parameters is interdependent on the wider electrical power system design and technology choice. This includes consideration of the influence of common-mode capacitances (parasitic and filter). The interdependencies between the choice of power converter topology, switching frequency and sink design with CM filter design and hence charging current also cannot be overlooked.

If the CFRP resistance is 25 Ω, and P_{thresh} is set to be 80 W, considering a nominal system frequency of 400 Hz and phase to ground voltage of 230 V, the charging capacitance will be set to be 1.03 μF, with R_{HRG} at 128.6 Ω. If the capacitance linked to ground cannot be limited to this threshold value, then a possible option may be to increase $R_{HRG.}$ Alternatively, it may be possible to design the CFRP such that R_{CFRP} has a minimum value to ensure that the fault current is not high enough to cause degradation. The resistance of the CFRP is sensitive to layup, cross-sectional area of conduction and panel size. However, the thermal response of the new CFRP configuration must be investigated to ensure that localized thermal response does not increase temperature above the resin glass transition temperature.

In addition, if the minimum value of R_{CFRP} is increased, or if R_{HRG} is decreased, a further consideration is that the method of detection presented relies on the spectral analysis of the neutral to ground voltage (V_{NG}). The magnitude of V_{NG} is directly proportional to the ratio of R_{HRG} to the sum of R_{HRG} and R_{CFRP}, and thus the magnitude of the frequency spectra. The limit for how high R_{CFRP} can be relative to R_{HRG} will depend on the level of noise on the ground plane. Further investigation is needed to investigate whether this variation in the spectra magnitude on a noisy, vibrating aircraft electrical power system would make it difficult to detect and locate a fault.

VII. Conclusions

Implementing a high resistance grounding topology may offer a way to reliably detect higher resistance faults through CFRP on an MEA EPS. This provides an opportunity to integrate CFRP with the EPS, enabling the conduction of currents under faulted conditions. Assuming that the range of electrical resistances that CFRP may add to the fault path of a rail to ground fault is known, an integrated approach to EPS system design can be taken to ensure that the heat dissipated within CFRP before a fault is detected and isolated, does not result either in the glass transition temperature of the resin being reached or the local environment being excessively heated. However, this may also result in implications for the wider electrical power system design: firstly considering the capacitive connections to ground, secondly the implications of over voltages.

The fault detection method proposed is based on spectral analysis of the neutral to ground voltage over R_{HRG}. This has been demonstrated using a simulation model which does not include all the parasitic capacitances and common-mode filters, or include noise that would be present in an aircraft environment. Hence hardware validation of the method is required to demonstrate capability of the method in a non-idealised set-up.

Linked to this, if the CFRP structure is to be truly integrated with the EPS, then further consideration of the common-mode currents and their circulation in CFRP must be undertaken. Even if these currents are not sufficiently high to result in localized heating of CFRP, they may contain high frequency components which may require appropriate EMC shielding.

Finally, if the grounding and fault detection strategy presented is extended to proposed hybrid-electric aircraft, the impact of the expected higher voltages (kV range) and frequencies will increase the value of *3Ico*. Changes in converter topologies for multilevel converters may result in higher parasitic capacitances. Ultimately, this may increase the size of the grounding resistance, which may help reduce the fault current.

Acknowledgments

This research undertaken as part of the Rolls-Royce University Technology Centre programme.

References

[1] B. Sarlioglu and C. T. Morris, “More Electric Aircraft: Review, Challenges, and Opportunities for Commercial Transport Aircraft,” *IEEE Trans. Transport. Electrification*., Vol. 1, No. 1, pp. 54–64, Jun. 2015. Doi: 10.1109/TTE.2015.2426499

[2] M. Terorde, H. Wattar, and D. Schulz, “Phase Balancing for Aircraft Electrical Distribution Systems,” *IEEE Trans. Aerosp. Electron. Syst*., Vol. 51, No. 3, pp. 1781–1792, Jul. 2015. Doi: 10.1109/TAES.2015.140031

[3] A. Piche, D. Andissac, I. Revel, and B. Lepetit, “Dynamic Electrical Behaviour of a Composite Material During a Short Circuit,” in *Proc. EMC Europe*, 2011, pp. 128–132.

[4] C. E. Jones et al., “Electrical Model of Carbon Fibre Reinforced Polymers for the Development of Electrical Protection Systems for More-Electric Aircraft,” in *Proc. 18th Eur. Conf. Power Electron. Appl*., Sep. 2016, pp. 1–10.

[5] “AC 43.13-2B – Acceptable Methods, Techniques, and Practices – Aircraft Alterations”, Federal Aviation Administration, 2008.

[6] “Lightning and Surge Protection, Grounding, Bonding and Shielding Requirements for Facilities and Electronic Equipment”, Federal Aviation Administration Standard 019e, 2005.

[7] S. M. Braden, M. J. Doherty, and S. M. Scott, “*Current return network*,” U.S. Patent 8 031 458 B2, Oct. 4, 2011.

[8] C. Lochot and D. Slomianowski, “A350 XWB electrical structure network,” *Airbus Tech. Mag*., Vol. 53, No. 53, pp. 20–25, Jan. 2014.

[9] “Integrated Accessories Raft System (ENABLES)”, Aerospace Technology Institute, 2016, [Online] https://www.ati.org.uk/wp-content/uploads/2017/09/110124_Integrated-Accessories-Raft-System-ENABLES-final.pdf [retrieved 18 June 2019].

[10] C.E. Jones et al, “Electrical and Thermal Effects of Fault Currents in Aircraft Electrical Power Systems with Composite Aerostructures”, *IEEE trans. Transportation Electrification*, Vol. 4, Issue 3, pp. 660-670, 2018. Doi: 10.1109/TTE.2018.2833838

[11] “MIL HDBK 274A Electrical Grounding for Aircraft Safety”, US Department of Defense, 2011.

[12] E. Kandare et al, “Improving the Through-Thickness Thermal and Electrical Conductivity of Carbon Fibre/Epoxy Laminates by Exploiting Synergy Between Graphene and Silver Nano-inclusions”, *Composites Part A: Applied Science and Manufacturing*, Vol. 69, pp. 72-82, 2015. Doi: 10.1016/j.compositesa.2014.10.024

[13] “IEEE recommended practice for grounding of industrial and commercial power systems (IEEE “Green Book”)”, *IEEE Std 142 – 2007*, IEEE, 2007.

[14] F. Jullien, “Cahiers Techniques no. 178: The IT earthing system (unearthed neutral) in LV”, *Schneider Electric*, 1999.

[15] I. Cotton et al, “Design Considerations for Higher Electrical Power System Voltages in Aerospace Vehicles”, *IEEE International Power Modulator and High Voltage Conference,* pp. 57 – 61, 2016.

[16] C. Bowman, J.L. Felder and T. Marien, “Turbo- and Hybrid-electrified aircraft propulsion concepts for commercial transport”, in *Proc. AIAA/IEEE Electric Aircraft Technologies Symposium*, 2018.

[17] C. Meijer, J. van der Ven and R. Ross, “EMC and Electrical Safety On-Board Ships”, in *Proc. International Symposium of Electromagnetic Compatibility*, 2013.

[18] T. Baldwin and F. Renovich, “Analysis of Fault Locating Signals for High-Impedance Grounded Systems”, *IEEE Trans. Industry Applications*, Vol.38, no. 3, 2002. Doi: 10.1109/TIA.2002.1003434

[19] M. Sztykiel, S. Fletcher, P. Norman, S. Galloway, G. Burt, "Modular and Reconfigurable Transient Modeling and Simulation Design Support Tool for MEE/MEA Power Systems", *Proc. SAE Aerosp. Syst. Technol. Conf.*, pp. 1-14, 2016.

[20] L. R. Lewis, B. H. Cho, F. C. Lee, B. A. Carpenter, "Modeling Analysis and Design of Distributed Power Systems", *Proc. 20th Annual. IEEE Power Electron. Spec. Conf.*, vol. 1, pp. 152-159, Jun. 1989.

[21] J. J. White, "Power Feeder Shielding for Electromagnetic Protection", U.S. Patent 9036323 B1, May 2015.

[22] M. Hartmanm, H. Ertl and J. W. Kolar, “EMI Filter Design for High Switching Frequency Three-Phase/Level PWM Rectifier Systems”, *25th Annual IEEE Applied Power Electronics Conference and Exposition*, 2010.

[23] 787 No-bleed systems, *Boeing AERO Magazine*, 2007.

[24] J. Hu, L. Wei, J. McGuire and Z. Liu, “Flux Linkage Detection Based Ground Fault Identification and System Diagnosis in High-Resistance Grounding Faults”, *IEEE Trans. on Industry Applications*, Vol. 53, No. 3, pp. 2967 -2975, 2017. Doi: 10.1109/TIA.2016.2621048

[25] G. Skibinski et al, “Part II: Application Guidelines for High Resistance Grounding of Low-Voltage Common AC-Bus and Common DC-Bus PWM Drive Systems”, *IEEE Trans. on Industry Applications*, Vol. 51, No. 2, pp. 1385 – 1397, 2015. Doi: 10.1109/TIA.2014.2363074

[26] A.P. Mouritz, “Introduction to Aerospace Materials”, Woodhead Publishing Ltd, UK, 2012

[27] J. Pou et al, “Fast-Processing Modulation Strategy for the Neutral-Point-clamped Converter with Total Elimination of Low-Frequency Voltage Oscillations in the Neutral Point”, *IEEE Trans. on Industrial Electronics*, Vol. 54, No. 4, pp. 2288 – 2294, 2007. Doi: 10.1109/TIE.2007.894788

[28] M. Schweizer, T. Friedli and J. W. Kolar, “Comparative Evaluation of Advanced Three-Phase Three-Level Inverter/Converter Topologies Against Two Level Systems”, *IEEE Trans. on Industrial Electronics*, Vol. 60, No. 12, pp. 5515 – 5527, 2013. Doi: 10.1109/TIE.2012.2233698

[29] G. Skibinksi et al, “Part 1: Application Guidelines for High Resistance Grounding of Low Voltage Common AC Bus and Common DC Bus PWM Drive Systems”, in *Proc. IEEE pulp and paper industry technical conference*, 2008.